

# Selective Deuteration Improves the Affinity of Adenosine A<sub>2A</sub> Receptor Ligands – A Computational Case Study with Istradefylline and Caffeine

Lucija Hok and Robert Vianello\*

Laboratory for the Computational Design and Synthesis of Functional Materials, Division of Organic Chemistry and Biochemistry, Ruđer Bošković Institute, 10000 Zagreb, Croatia.

\*Corresponding author. Email: robert.vianello@irb.hr

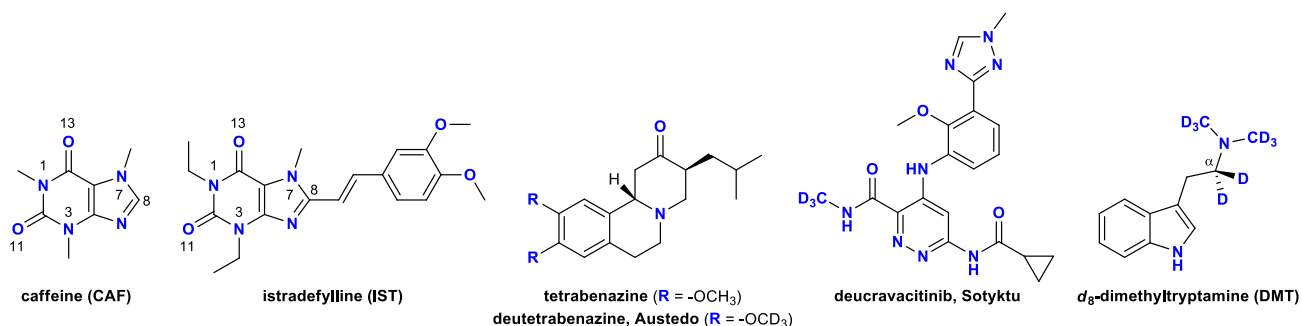
## ABSTRACT

We used a range of computational techniques to assess the effect of the selective C–H deuteration on the antagonist istradefylline affinity for the adenosine A<sub>2A</sub> receptor, which was discussed relative to its structural analogue caffeine, a well-known and likely the most widely used stimulant. The obtained results revealed that smaller caffeine shows large receptor flexibility and exchanges between two distinct poses, which agrees with crystallographic data. In contrast, the additional C8-*trans*-styryl fragment in istradefylline locks the ligand within a uniform binding pose, while contributing to the affinity through the C–H⋯π and π⋯π contacts with surface residues, which, together with its much lower hydration prior to binding, enhances the affinity over caffeine. In addition, the aromatic C8-unit shows a higher deuteration sensitivity over the xanthine part, so when both of its methoxy groups are *d*<sub>6</sub>-deuterated, the affinity improvement is –0.4 kcal mol<sup>–1</sup>, which surpasses the overall affinity gain of –0.3 kcal mol<sup>–1</sup> in the perdeuterated *d*<sub>9</sub>-caffeine. Yet, the latter predicts around 1.7-fold potency increase, being relevant for its pharmaceutical implementations, but also those within the coffee and energy drinks production industries. Still, the full potential of our strategy is achieved in the polydeuterated *d*<sub>19</sub>-istradefylline, whose A<sub>2A</sub> affinity improves by –0.6 kcal mol<sup>–1</sup>, signifying a 2.8-fold potency increase that strongly promotes it as a potential synthetic target. This knowledge supports deuterium application in the drug design, and while the literature already reports about over 20 deuterated drugs currently in the clinical development, it is easily foreseen that more examples will hit the market in the years to come. With this in mind, we propose that the devised computational methodology, involving the ONIOM division of the QM region for the ligand and the MM region for its environment, with an implicit quantisation of nuclear motions relevant for the H/D exchange, allows fast and efficient estimates of the binding isotope effects in any biological system.

## INTRODUCTION

Adenosine receptors (ARs) belong to the class A subfamily of G protein-coupled receptors (GPCRs) that consist of four subtypes, A<sub>1</sub>, A<sub>2A</sub>, A<sub>2B</sub>, and A<sub>3</sub>. Based on sequence similarity and G protein-coupling specificity, ARs can be divided into two groups: A<sub>1</sub>R and A<sub>3</sub>R that share 49% sequence identity and predominantly couple to G proteins of the Gα<sub>i/o</sub> family leading to the inhibition of cAMP production by adenylate cyclase, whereas the sequences of A<sub>2A</sub>R and A<sub>2B</sub>R are 59% identical and they couple to Gα<sub>s</sub> achieving the opposite effect.<sup>1</sup> ARs are ubiquitously expressed in many cell types and are associated with several disorders including inflammatory processes (A<sub>2A</sub> and A<sub>3</sub>); respiratory pathological events such as allergic asthma (A<sub>2B</sub> and A<sub>3</sub>); vascular diseases (A<sub>2A</sub>); as well as arrhythmias and stroke (A<sub>1</sub>).<sup>2</sup>

Among all subtypes, adenosine A<sub>2A</sub> receptor is of particular interest as it is one of the best structurally characterised GPCRs at the atomic level, with more than 30 crystal structures published to date.<sup>3</sup> Besides that, A<sub>2A</sub>AR inactivation ameliorates neuropsychiatric and neurodegenerative symptoms, which led to these antagonists emerging as promising non-dopaminergic alternatives in the Parkinson's disease treatment, and have attracted much attention in the clinical development, particularly after istradefylline (Scheme 1) has been approved in Japan and the USA.<sup>4</sup> Although the molecular mechanism behind the A<sub>2A</sub>AR antagonism is far from certain, there are reports showing that ARs can undergo homo- and heterodimerisation or even oligomerisation, in particular with D<sub>2</sub>, mGluR<sub>5</sub>, CB<sub>1</sub>, and A<sub>1</sub>, which may be correlated with a wide range of neurological symptoms. Therefore, A<sub>2A</sub>AR antagonists are gaining importance for the treatment of Huntington's disease, epilepsy, and cerebral ischemia, but also in improving tumour inhibition.<sup>5</sup>



**Scheme 1.** Chemical structures and atom labelling for systems discussed in the text.

Adenosine A<sub>2A</sub> receptor antagonists have been usually classified as xanthine or nonxanthine derivatives, the latter including a large class of systems having tri-, bi- and monocyclic scaffolds with various substituents.<sup>6</sup> Besides structural modifications, the past few years have witnessed an emerging trend in the use of deuteration in the medicinal chemistry as the most conservative example of the bioisosterism. The latter was particularly triggered in 2017, after the FDA granted market approval for the first deuterium-labelled drug – VMAT2 inhibitor Austedo (Scheme 1) for the treatment of chorea associated with the Huntington's disease. This represented a major milestone in the advancement of this approach and its clinical and financial viability, and provided a framework for the approval of other deuterium enriched drugs.<sup>7</sup> Exchanging the six methoxy H atoms with D, alters Austedo metabolism, increasing its safety and tolerability by conferring upon it an extended half-life and a more stable plasma concentration, allowing a reduction of the recommended daily dosage in half relative to its non-deuterated tetrabenazine analogue.<sup>8,9</sup> Very recently, in September 2022, another deuterated drug, deucravacitinib (Scheme 1), was registered in the USA as a first-in-class selective allosteric tyrosine kinase 2 inhibitor and the innovation in oral treatment for moderate-to-severe plaque psoriasis.<sup>10</sup> To ensure the selectivity of the methyl amides *in vivo*, deuterium was

incorporated into the methyl group to block an *N*-demethylation metabolic pathway that generated a less selective primary amide metabolite. Unlike many other deuterated examples of improved pharmacokinetic properties that rely on already existing drug developmental candidates or marketed medicines, the novelty in this approach is that deuterium was incorporated during *de novo* design and optimisation process,<sup>11</sup> which represents another crucial milestone in the development of deuterium-enriched drugs. In the field of xanthines, a very recent report showed that *d*<sub>9</sub>-caffeine with three deuterated methyls, exhibits prolonged systemic and brain exposure following oral administration.<sup>12</sup> Specifically, it revealed that despite a lower lipophilicity, *d*<sub>9</sub>-caffeine maintains the ability to cross the blood-brain barrier, is negative in both the Ames's bacterial reverse mutation assay and mammalian cell micronucleus assay, such that it may be considered non-genotoxic, and retains most of its physico-chemical properties similar to the non-deuterated analogue, thereby suggesting that most of their other drug-likeness features would likely be similar. In fact, this was subsequently confirmed in a double-blind, randomized, two-part, two-period crossover study on humans,<sup>13</sup> which revealed that *d*<sub>9</sub>-caffeine caused no adverse events of insomnia or clinically significant ECG or vital signs findings, promoting it as a safe and well-tolerated alternative to caffeine.

In general, deuterated drugs have proved useful in studying isotope effects, in permitting a better understanding of the drug action mechanisms, and in elucidating metabolic and biosynthetic pathways. The most important difference between the two isotopes manifests itself as a shortening of the covalent C–D bond relative to C–H, very often causing an increase in stability to metabolic oxidative processes, a phenomenon known as the kinetic isotope effect. Namely, D has twice the mass of H leading to a reduced vibrational stretching frequency and, therefore, lower ground state energy. This is accompanied by a higher activation energy required to reach the transition state for its bond cleavage and a slower reaction rate.<sup>14</sup> Therefore, the most straightforward application of deuterium substitution is to slow down drug metabolism, especially cytochrome P450 (CYP450)-mediated transformations that rely on C–H/D bond cleavage,<sup>15</sup> which allows prolonged drug exposure, thereby permitting lower dosages and less frequent applications. One illustrative recent example is afforded by *N,N*-dimethyltryptamine (DMT, Scheme 1) in the treatment of psychiatric and neurological disorders, which exerts its activity by activating a variety of neuroreceptors, yet it is rapidly metabolised by MAO A through the rate-limiting hydride abstraction from  $\alpha$ -methylene adjacent to amine.<sup>16–18</sup> In this context, a recent report showed that *d*<sub>6</sub>-DMT with the deuterated –NMe<sub>2</sub> group distant from the metabolic soft spot, retains the low half-life of the parent drug, while *d*<sub>8</sub>-DMT, additionally having the  $\alpha$ -CD<sub>2</sub> moiety, increases it by 2.1-fold,<sup>19</sup> clearly due to a hindered MAO A conversion.

In this context, although deuteration still is most often exploited to improve the pharmacokinetic features of drug candidates when incorporated at sites relevant to metabolic conversion, the differences in physico-chemical properties between H and D can have a notable impact on the ligand binding to the receptor as well. Compared to hydrogen, deuterium displays a smaller molar volume (by 0.140 cm<sup>3</sup> mol<sup>-1</sup> per atom), is less lipophilic ( $\Delta \log P_{\text{oct}} = -0.006$ ), and typically exhibits slightly different pK<sub>a</sub> values.<sup>14,20</sup> Since the ligand binding to a biological macromolecule is a process comparable in some respects to the extraction of a solute from water into a media of lower polarity, the rate and extent of that interaction are broadly related to the ligand lipophilicity,<sup>21</sup> which means that the H/D substitution may in some cases have marked biological consequences.<sup>22–25</sup> Along these lines, our earlier work revealed modified affinities of several histamine H<sub>2</sub> receptor agonists and antagonists following the nonselective incubation in D<sub>2</sub>O. Specifically, a joint experimental and computational study reported increased affinities for agonists histamine ( $\Delta \Delta G_{\text{BIND}} = -0.75$  kcal mol<sup>-1</sup>)<sup>26</sup> and 4-methylhistamine ( $\Delta \Delta G_{\text{BIND}} = -0.49$  kcal mol<sup>-1</sup>), and lower for 2-methylhistamine ( $\Delta \Delta G_{\text{BIND}} = 2.08$  kcal mol<sup>-1</sup>), while no change was observed for antagonists cimetidine and famotidine.<sup>27</sup> This underlines an important conclusion that the deuteration effect on receptor affinities is not general and cannot be predicted in a simple way. Instead, it needs to be individually examined, yet therapeutic improvements can be achieved.

With this in mind, here we employed a range of computational techniques, involving docking studies, classical molecular dynamics simulations, and quantum-chemical as well as combined quantum-mechanics/molecular-mechanics ONIOM calculations, to provide a more precise insight into the effect of the selective deuteration on the potency of adenosine A<sub>2A</sub> receptor antagonists caffeine and istradefylline (Scheme 1). Both ligands share xanthine skeleton characteristic of various A<sub>2A</sub>AR antagonists, but show dissimilarity in the selectivity towards different AR subtypes: caffeine possesses roughly equally low affinities for all adenosine receptors, while istradefylline, due to the additional C8-*trans*-styryl fragment, is highly selective for A<sub>2A</sub>AR (Table 1),<sup>28</sup> with affinities exceeding those for caffeine, thereby making it an excellent candidate for further development. As a first-in-class drug, istradefylline has been shown to be effective in improving the "wearing-off" phenomenon in patients with Parkinson's disease (PD) on levodopa-containing therapy.<sup>4</sup> Namely, the majority of current PD medications aim to restore dopamine signalling and thereby reduce the severity of the motor symptoms by directly replacing dopamine with *L*-DOPA or by targeting related biological systems such as monoamine oxidase B, catechol *O*-methyl-transferase and dopamine transporters or receptors. Despite their benefit at the beginning, their use is associated with a loss of efficacy over time (fluctuations in response such as "wearing-off") as well as many undesirable side effects (dyskinesia, hallucinations, "on-off") that become more severe and problematic with the prolonged treatment. In addition, the most non-motor manifestations, including neuropsychiatric conditions (depression, cognitive decline, sleep disturbance) and postural instability that frequently accompany PD, are only partially responsive to dopaminergic drugs, leaving a high degree of unmet need which offer an opportunity for discovering new targets and addressing a wider spectrum of symptoms.<sup>6,29</sup> Based on preclinical and clinical data, the majority of novel approaches focus precisely on the selective A<sub>2A</sub>R antagonism, which shows great potential in the treatment of both motor and non-motor disorders as well as indications for disease modification, however, the full potential of this drug class remains to be explored. Moreover, istradefylline already represents the starting point towards even safer and more potent structural analogues.<sup>30</sup> The presented analysis is likely to contribute to the identification of structural and electronic features of the studied ligands important for receptor antagonism with the aim to provide the molecular interpretation of the observed affinity differences upon deuteration.

**Table 1.** Experimentally measured  $K_i$  values for caffeine and istradefylline towards the adenosine receptor subtypes as taken from refs. 5,31.

receptor subtype	$K_i$ (nM)	
	caffeine	istradefylline
A <sub>1</sub>	10.700	841
A <sub>2A</sub>	23.400	5.7
A <sub>2B</sub>	33.800	> 10.000
A <sub>3</sub>	13.300	4.470

## RESULTS AND DISCUSSION

### Molecular Docking Simulations

To determine the relevant caffeine and istradefylline binding positions, we conducted docking simulations employing the inactive structure of the adenosine A<sub>2A</sub> receptor obtained by homology modelling. Based on the docking scores, the most favourable poses of both ligands correspond to the orthosteric binding site located in the upper third region of the 7TM core between the third and sixth  $\alpha$ -helices (Figure 1).<sup>2</sup> Superposition of the identified ligand poses to the crystal structure with caffeine (PDB entry: 5MZP)<sup>1</sup> reveals that the istradefylline xanthine ring occupies the binding mode A in which O13 establishes the hydrogen bond with Asn253<sup>6.55</sup>, while the orientation of O11 towards His278<sup>7.43</sup> enables the formation of water-mediated interactions. In contrast, the caffeine docking pose matches up with the mode B where O11 and O13 locations are approximately interchanged. The fused rings of both ligands are engaged in the  $\pi$ ·· $\pi$  hydrophobic interactions with Phe168<sup>45.52</sup>, characteristic for the polyheteroaromatic scaffolds within a planar and narrow cavity of the binding pocket. This confirms the validity of the employed docking procedure, being further promoted by the calculated affinities of  $-5.7$  kcal mol<sup>-1</sup> for caffeine and  $-7.6$  kcal mol<sup>-1</sup> for istradefylline that are found in a reasonable qualitative agreement with the experimental values of  $-7.7$ <sup>32</sup> and  $-11.2$  kcal mol<sup>-1</sup>,<sup>31</sup> respectively. In order to inspect receptor dynamics and conformational changes upon the ligands binding within the orthosteric site, we utilised the identified docking structures as starting points for MD simulations of the A<sub>2A</sub> receptor immersed in the membrane.<sup>33</sup>

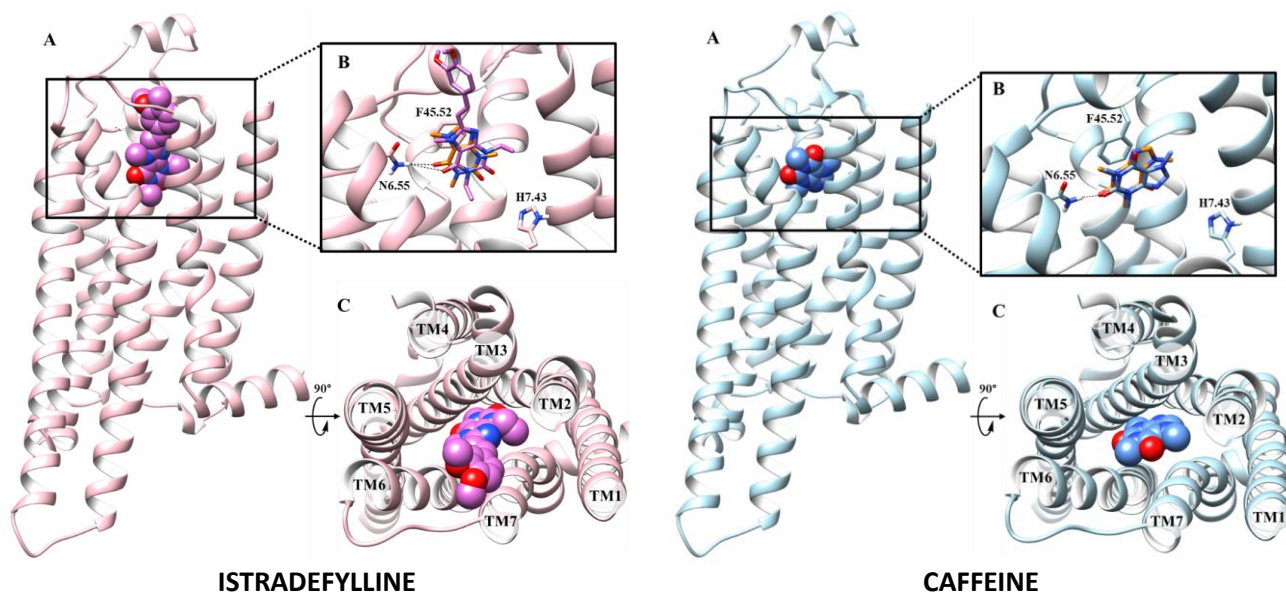


**Figure 1.** A) Side view of the most favourable binding pose of istradefylline (left) and caffeine (right) within the A<sub>2A</sub> receptor as predicted by molecular docking simulations. B) Superposition of the caffeine-bound crystal structures (PDB entry: 5MZP, in orange) with the relevant docking pose (in magenta) corresponding to the mode A for istradefylline and mode B for caffeine. Residues are labelled according to the Ballesteros-Weinstein numbering scheme. C) Extracellular view of the most favourable binding pose within the orthosteric site between TM3 and TM6  $\alpha$ -helices. ECL1 and ECL2 are omitted due to clarity.

## Molecular Dynamics Simulations

In order to examine  $A_{2A}$  receptor conformational changes following the antagonists orthosteric binding, we constructed three simulation models: one apo- $A_{2A}$ AR and two holo- $A_{2A}$ ARs based on the previously discussed docking analysis, all embedded in a homogeneous membrane consisting of 1,2-dioleoyl-*sn*-glycero-3-phosphocholine (DOPC). Apart from its important role in modelling the behaviour of biomembranes,<sup>34,35</sup> the choice of that particular bilayer is supported by the experimental and computational studies that suggest different phospholipid environments can act as positive, negative or neutral allosteric modulators of the class A GPC receptors.<sup>36–39</sup> Positive effects are mainly mediated by the hydrogen bonding contacts between the protein and phospholipid headgroups within the negatively charged DOPG. The lack of such groups in DOPC allows a slow destabilisation of the active state making it a neutral allosteric modulator (Figure 2).

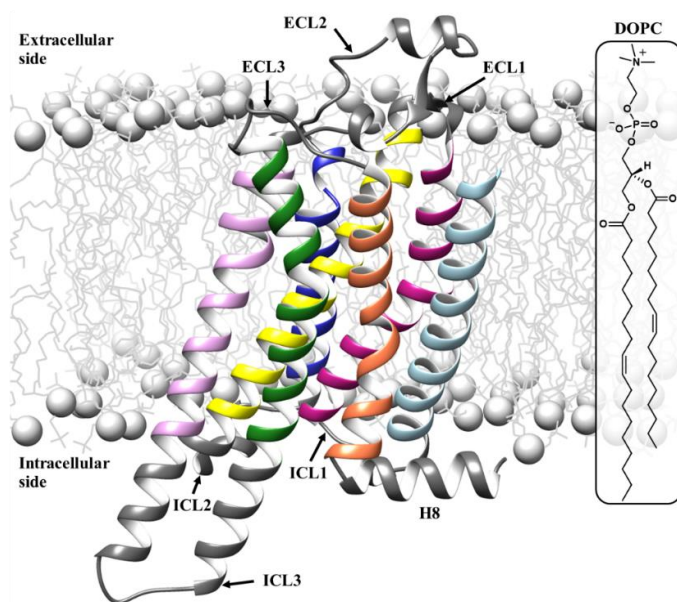


**Figure 2.** Initial structure for MD simulations of the apo- $A_{2A}$  adenosine receptor immersed in the DOPC membrane with transmembrane domains differently coloured: TM1 in light blue, TM2 in magenta, TM3 in yellow, TM4 in dark blue, TM5 in light purple, TM6 in green, and TM7 in orange. Intra- and extracellular loops, as well as the helix 8, are represented in dark grey and labelled separately, while DOPC molecules are shown in light grey with phospholipid headgroups represented as spheres. The inset image shows the structure of a single DOPC molecule.

Unbiased 600 ns of MD simulations were performed in quadruplicate, and the validity of this approach was justified through the corresponding RMSD graphs of the protein backbone atoms, which reveal converged trajectories (Figure S1). To study the antagonist induced  $A_{2A}$ AR conformational dynamics, we mainly focused on highly conserved motifs and secondary loop structures, whose rearrangements modify the receptor functionality, thus ensuring active, intermediate or inactive states. Among them, the "ionic lock", the "rotamer toggle switch" and specific transmembrane domain movements have been identified as characteristic structural determinants between active and inactive protein conformations in the GPCR family. The ionic lock pertains to the electrostatic interaction between Arg102<sup>3,50</sup> of the conserved D[E]RY motif (D<sup>3,49</sup>, R<sup>3,50</sup>, Y<sup>3,51</sup>) and Glu228<sup>6,30</sup>, thus forming a link between intracellular ends of TM3 and TM6 which

stabilises the inactive state. For apo- $A_{2A}$ AR, MD simulations reveal that the ionic lock mainly remained preserved in all four replicas with the average hydrogen bond occurrence between Arg102<sup>3,50</sup> and Glu228<sup>6,30</sup> of 73%, and the distance between their  $C_{\alpha}$  atoms of 8.2 Å, being almost identical to the inactive crystal structure distance of 8.1 Å (PDB entry: 5IU4).<sup>39</sup> In both holo-receptors, the stability of the R<sup>3,50</sup>...E<sup>6,30</sup> salt bridge is even more pronounced with the average hydrogen bond occurrence of 85% and the distance between  $C_{\alpha}$  atoms of 7.5 Å for caffeine-bound  $A_{2A}$ AR, as well as 83% and 7.4 Å for istradefylline-bound  $A_{2A}$ AR, respectively (Table S1, Figures S2, S3). Furthermore, considering that upon activation the most significant changes also occur at the cytoplasmic ends of TM5 and TM7, we monitored their fluctuations relative to the TM3. In both apo- and holo- $A_{2A}$ ARs, the measured average distances closely match those observed in the crystal structure of the inactive state,<sup>39</sup> which confirms the stability of the inactive receptor conformation in all three studied models (Table S1, Figures S2, S3). For the sake of comparison, an outward movement of TM6 by 5 Å breaks the ionic lock in the active state, which is, along with outward and inward lateral motions of TM5 by 7 Å and TM7 by 4 Å, thought to prime the receptor for the G protein coupling.<sup>40,41</sup> Analogous to the ionic lock, a highly conserved CWxP motif (C<sup>6,47</sup>, W<sup>6,48</sup>, L<sup>6,49</sup>, P<sup>6,50</sup>) contains Trp246<sup>6,48</sup> whose orientation had been hypothesised as a marker for the activation state of GPCRs.<sup>2</sup> Namely, agonist binding deep into the pocket leads to a steric clash with Trp246<sup>6,48</sup> that causes the conformational switch from *gauche*(+) ( $\chi_1 = -60^\circ$ ) to *trans* ( $\chi_1 = 180^\circ$ ), and subsequently induces positional changes of TM5 and TM6. Over the all four replicas of apo-, caffeine-bound and istradefylline-bound  $A_{2A}$ AR simulations, we noticed that Trp246<sup>6,48</sup> maintains the most stable *gauche*(+) form characteristic of the inactive state in which the gamma side chain atom is opposite to the main chain carbonyl group when viewed along the  $C_{\beta}$ - $C_{\alpha}$  bond, with the average  $\chi_1$  values of  $-75^\circ$ ,  $-72^\circ$  and  $-69^\circ$ , respectively (Figure S4). All of this confirms the inactive state of the  $A_{2A}$  receptor as predominant in all three cases and the antagonistic features of both ligands during employed MD simulations.

Regarding the behaviour of the extracellular part of the receptor, the most pronounced flexibility can be observed in the ECL2 loop which, due to its size and structural diversity, proved to be the most functionally significant of the three ECLs (Figure S1). Recent literature has implicated ECL2 in many key aspects of receptor function, such as ligand selectivity and kinetics,<sup>42</sup> as well as direct involvement in the binding as part of orthosteric and allosteric sites, thereby allowing it to control a complex process of signal transduction, including biased signalling and constitutive activity.<sup>43,44</sup> Comparing RMSD graphs of the backbone atoms for the entire protein to those from the ECL2 loop, we perceived that receptor conformational changes most likely come from the large flexibility of the ECL2 loop, which is especially favoured in the apo-state (Figure S5). This was confirmed by the average fluctuation of ECL2 residues (RMSF) across the four replicas with values of  $98.4 \pm 4.5$  Å in apo- $A_{2A}$ AR, and  $102.3 \pm 5.6$  Å and  $90.53 \pm 2.7$  Å in caffeine- and istradefylline-bound  $A_{2A}$ AR simulations, respectively (Figure S1). The higher stability achieved in the latter holo-model is ascribed to the 3,4-dimethoxyphenyl group of istradefylline, which stabilises ECL2 by occupying the allosteric subsidiary site closer to the surface and located between  $\alpha$ -helices H1, H2 and H7,<sup>40</sup> while the smaller caffeine binds only into a deeply buried orthosteric pocket allowing the loop flexibility comparable to that of apo- $A_{2A}$ AR. Nevertheless, the salt bridge between Glu169 on ECL2 and His264 on ECL3, which is known to affect the ligand kinetics by acting as a binding site lid,<sup>40</sup> is equilibrated between the formed and broken interaction with a much lower occurrence in the apo-receptor (approximately 26% of the simulation time) compared to both holo-models (46% in CAF- $A_{2A}$ AR and 40% in IST- $A_{2A}$ AR) (Figure S6). The relatively persistent electrostatic bond stabilises the position of the antagonists within the binding pocket and prolongs their residence time by slowing the off-rate from the receptor.

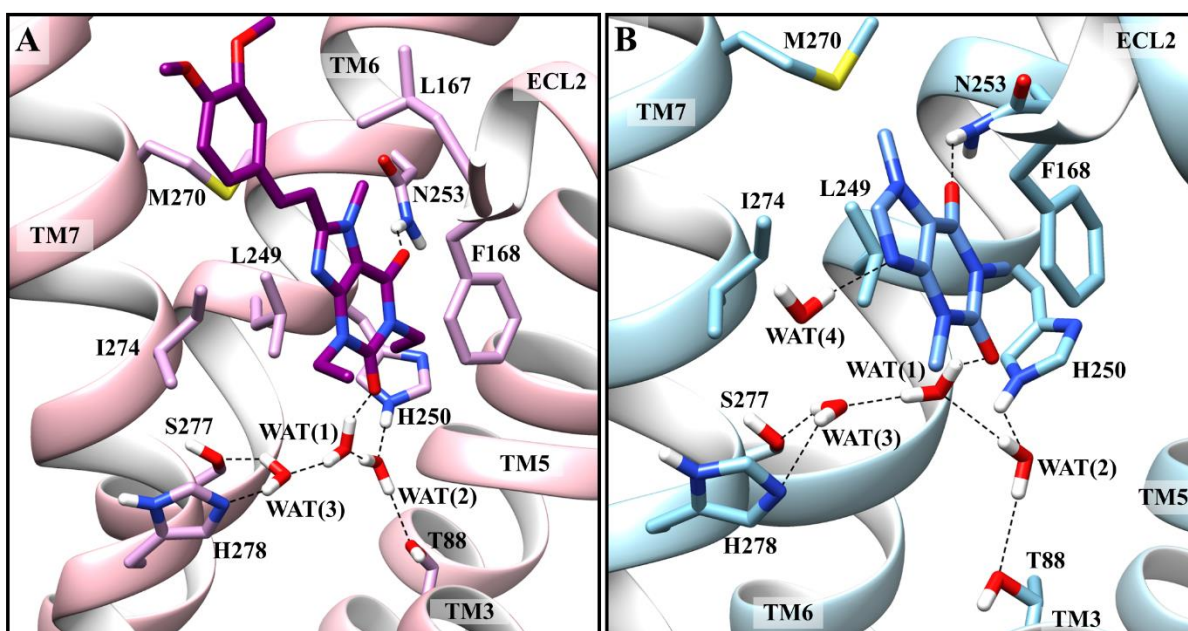


**Figure 3.** Representative structures of A) istradefylline and B) caffeine within the  $A_{2A}AR$  binding site with the most dominant residues and water bridge molecules individually labelled, as obtained from the MD simulations.

The most prominent interactions formed among antagonists and the residues within the binding pocket were identified by the MM-GBSA approach, and their individual contributions to the affinities are given in Tables S2 and S3. Caffeine and istradefylline share a common xanthine moiety that in both cases form  $\pi\cdots\pi$  stacking interactions with Phe168<sup>ECL2</sup> on one side and  $CH\cdots\pi$  interactions with Leu249<sup>6.51</sup> on the other, which makes these two residues the most dominant for the binding (Tables S2–S3, Figures 3, S7, S8). Specifically, caffeine establishes the mentioned  $\pi\cdots\pi$  contacts during two thirds of the simulation time (68%), while the  $CH\cdots\pi$  interactions were observed in 43% of structures. In contrast, both hydrophobic interactions are more pronounced in istradefylline, 92% and 94%, respectively, thereby making significant contributions to its higher  $A_{2A}AR$  affinity. Given that two different binding modes were obtained by docking simulations as the most favourable, A for istradefylline and B for caffeine, it is to be expected that O13 in the first case and O11 in the latter form hydrogen bonds with the N $\delta$ 2 atom of Asn253<sup>6.55</sup>. However, MD analysis of the observed interactions reveals a greater positional freedom of the smaller caffeine within the binding site, which is reflected in a higher average RMSF value of  $2.37 \pm 0.16$  Å compared to  $2.05 \pm 0.21$  Å for istradefylline (Figure S1). As a result, the caffeine xanthine core rotates and forms hydrogen bonds through both O11 and O13 atoms, assuming 49% and 25% of the simulation time, respectively, which confirms the experimentally observed equivalence of the two crystallised modes (Figure S9).<sup>1</sup> On the other hand, these interactions are also more significant in istradefylline, which, due to a more uniform binding pose, forms the mentioned hydrogen bonding contacts only with its O13 site that are observed in 86% of the recorded structures. Although these bonds are considered pivotal to the ligand binding,<sup>45</sup> it is interesting to observe that residues such as, already mentioned Phe168<sup>ECL2</sup> and Leu249<sup>6.51</sup>, as well as Met270<sup>7.35</sup>, Ile274<sup>7.39</sup>, Met177<sup>5.38</sup>, His250<sup>6.52</sup> and His278<sup>7.43</sup> jointly, and some of them individually, surpass the Asn253<sup>6.55</sup> contribution, thus confirming the suggestion that hydrophobic groups dictate the strength of xanthines connection with  $A_{2A}AR$ s (Tables S2 and S3).<sup>1</sup> Their importance stems not only from van der Waals interactions, but also from their involvement



in the water-mediated hydrogen bond network, whose flexibility and the ability to reorganise can optimise ligand binding<sup>46</sup> and play an important role in the transition to a fully active receptor state.<sup>47</sup> Our simulations with holo-A<sub>2A</sub>ARs reveal that the first water molecule (1) indirectly connects O11 with Thr88<sup>3.36</sup> and His250<sup>6.52</sup> through the second water (2), as well as with Ser277<sup>7.42</sup> and His278<sup>7.43</sup> through the third water (3) (Figure 3). In addition, His250<sup>6.52</sup> further stabilises antagonists by the hydrophobic CH $\cdots$  $\pi$  interactions with the istradefylline N1-ethyl and all three caffeine *N*-methyls occasionally, due to their free rotation within the binding site (Figure S10). It is worth emphasising that the structural differences between agonists and antagonists come to the fore precisely in this part of the orthosteric pocket, since the existence of the ribose moiety allows adenosine to bind directly to S277<sup>7.42</sup> and H278<sup>7.43</sup> via the hydroxyl groups at positions C2 and C3, which suggests that the simultaneous engagement of these residues may be a key determinant of agonist activity.<sup>40,41,48</sup>

Due to an additional chemical moiety bound to the C8 site, istradefylline can exploit the subsidiary binding site located among TM1, TM2, and TM7 on the extracellular surface of the receptor. The aromatic ring of the 3,4-dimethoxyphenyl group achieves the strongest interactions with Leu167<sup>5.28</sup> (22% of structures) and Met270<sup>7.35</sup> (50% of structures) through CH $\cdots$  $\pi$  bondings, followed by contacts with Ile66<sup>2.64</sup>, Leu267<sup>7.32</sup>, Ala63<sup>2.61</sup>, Ser67<sup>2.65</sup>, Tyr271<sup>7.36</sup> and Tyr9<sup>1.35</sup>, similar to other antagonists (Table S3 and Figure S11).<sup>40,49</sup> Particularly important among them is Met270<sup>7.35</sup>, which was elucidated through mutagenesis studies to play a key role in establishing the ligand selectivity between A<sub>1</sub> and A<sub>2A</sub> receptors. Namely, the M270T mutation in A<sub>2A</sub>AR caused a decrease in the affinity of A<sub>2A</sub>AR-specific ligands, while at the same time it increased the affinity of those specific for A<sub>1</sub>AR.<sup>1,50</sup> Considering its position on the extracellular end of TM7, Met270<sup>7.35</sup> has been speculated to act as a "gatekeeper" regulating the orthosteric site ligand access that could have implications in the development of drugs that target individual AR subtypes with sufficient specificity to limit off-target side effects.<sup>40</sup>

In concluding this part, we can emphasise that the employed MD simulations and the subsequent MM-GBSA analysis consistently indicate a high flexibility of a smaller caffeine within the A<sub>2A</sub>R binding site, which is reflected in the ability of its carbonyl O11 and O13 atoms to exchange in forming hydrogen bonding contacts with Asn253<sup>6.55</sup>, but also in alternating significance of the receptor residues in the four independent MD replicas for its accommodation within the binding pocket (Table S2). This leads to a lower affinity between the two studied antagonists, and underlines an important message that an extensive ligand flexibility within the binding pocket can, unlike expected mobility to optimise contacts with protein residues and improve the binding, occasionally reduce the overall affinity. We observed a similar behaviour for histamine and its ring *N*-methyl derivative, where a higher flexibility of a smaller histamine within the metabolising MAO B enzyme facilitates unproductive active site orientations, resulting in a complete absence of its catalytic conversion.<sup>51</sup> In contrast, less flexible *N*-methylhistamine positions only in productive orientations leading to its fast metabolic oxidation to the corresponding aldehyde. Accordingly, the additional istradefylline C8-*trans*-styryl fragment serves the purpose of locking the ligand within a uniform binding pose, evident in only O13 interacting with Asn253<sup>6.55</sup>, and a more regular distribution of the crucial residues in all four replicas (Table S3). While doing that, the C8-aromatic unit predominantly interacts with Met270<sup>7.35</sup> that typically even surpasses the positive contribution from Asn253<sup>6.55</sup>, in line with other reports, underlying its importance for the istradefylline accommodation.<sup>52</sup>

### Combined QM and QM/MM Calculations

In order to computationally evaluate the effect of the selective antagonist deuteration, we carried out a series of calculations on different levels of theory, employing an implicit quantisation of C–H bonds as a method for studying the H/D isotope substitution.<sup>26,27</sup> Considering that antagonists primarily reside in the aqueous solution before reaching the receptor, we had to assess how deuteration affects both contributions to the total binding energy ( $\Delta E_{\text{BIND}}$ ), the one from the hydration of antagonists ( $\Delta E_{\text{HYDR}}$ ) and the other from their interaction with the receptor ( $\Delta E_{\text{INT}}$ ), as explained in the Computational Details section.

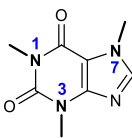
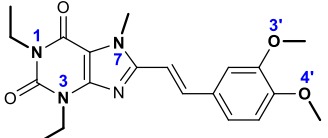
As mentioned, the deuterium substitution at C–H sites modifies their lipophilicity, an effect that can be divided into two parts, volume (or cavity) and polarity contributions, leading to changes in the interaction energy in which these bonds participate.<sup>21</sup> Since the overall binding isotope effect (BIE) comprises the hydration and protein interaction terms, it can, at the end, be either positive or negative, depending on the physico-chemical properties of the ligand and the host system.<sup>20</sup> As an illustrative example, Cherrah et al.<sup>24</sup> studied the binding of different caffeine deuterium isotopomers to human serum albumin by the equilibrium dialysis, and showed that  $K_a$  values for caffeine-1-CD<sub>3</sub> and caffeine-1,3,7-(CD<sub>3</sub>)<sub>3</sub> differed negligibly, while those for caffeine-3-CD<sub>3</sub>, caffeine-1,7-(CD<sub>3</sub>)<sub>2</sub>, and caffeine-3,7-(CD<sub>3</sub>)<sub>2</sub> were slightly lower than for the non-deuterated analogue. Relative to that, through the reversed-phase HPLC, Bechalany et al. showed that lipophilicity decreased when going from unlabelled caffeine to the three isomeric *d*<sub>3</sub>-caffeines, then to the three isomeric *d*<sub>6</sub>-caffeines, and finally to *d*<sub>9</sub>-caffeine. In addition, position-specific effects were also proven since caffeine-7-CD<sub>3</sub> experienced a smaller isotope effect than its 1- and 3-CD<sub>3</sub> isomers (Table S4).<sup>21</sup> These results indicate that the binding isotope effect is a complex phenomenon that cannot be interpreted only by changing the molecule lipophilicity, but rather depends on the intricate interplay between ligand behaviour in polar aqueous and nonpolar receptor environments, therefore, a thorough approach to examine the impact on affinity is required for each individual system.

Our ONIOM and DLPNO-CCSD(T) results are given in Table 2, which displays absolute values for  $\Delta E_{\text{HYDR}}$  and  $\Delta E_{\text{INT}}$  contributions to the total affinity ( $\Delta E_{\text{BIND}}$ ), and relative changes to the latter following deuteration of all H-atoms within a particular alkyl moiety ( $\Delta\Delta E_{\text{BIND}}$ ). The first appealing aspect is that both ONIOM and DLPNO-CCSD(T) methodologies accurately predict the higher affinity of istradefylline over caffeine, thereby agreeing with experiments. Although data for istradefylline are somewhat exaggerating the binding,  $-18.6 \text{ kcal mol}^{-1}$  within ONIOM[2] and  $-17.7 \text{ kcal mol}^{-1}$  within DLPNO-CCSD(T), relative to the experimental value of  $-11.2 \text{ kcal mol}^{-1}$ , it is interesting to observe an almost perfect agreement between ONIOM[2] calculated ( $-7.6 \text{ kcal mol}^{-1}$ ) and measured affinity ( $-7.7 \text{ kcal mol}^{-1}$ ) for caffeine, which lends some credence to the utilised ONIOM approach. Still, such a large general discrepancy between calculated and measured affinities is probably not surprising, and likely emerges as a consequence of the arbitrary nature of the subdivision among regions in the ONIOM[2] approach or the choice of the truncated receptor model in DLPNO-CCSD(T) calculations. Yet, unlike in ONIOM[1], which comes with a more straightforward QM/MM ligand-receptor separation, the former two methodologies were implemented because, apart from differences in  $\Delta\Delta E_{\text{BIND}}$  values that are in focus of our attention for the drug-design purposes, they allow the calculation of their contributions,  $\Delta E_{\text{INT}}$  and  $\Delta E_{\text{HYDR}}$ . The latter offer a powerful interpretation tool, since they reflect the intrinsic stability of a ligand within both the receptor interior and the aqueous solution preceding the binding, respectively. However, both values, together with their overall affinity ( $\Delta E_{\text{BIND}}$ ), should primarily be used to discuss ligand differences in relative terms.

When the contributions to  $\Delta E_{\text{BIND}}$  are considered, one arrives to interesting insights. The hydration energy,  $\Delta E_{\text{HYDR}}$ , which describes the stability of each ligand in the pure aqueous solution, is significantly higher for

caffeine. This is reasonable knowing that it is much more hydrophilic over istradefylline. Specifically, already when the common xanthine fragment is compared, caffeine bears three small methyl moieties on each of the three tertiary amines, which are replaced by two larger and more hydrophobic ethyl groups in istradefylline, let alone the fact that the additional C8-*trans*-styryl fragment is significantly aromatic and hydrophobic on its own. All of this justifies the higher  $\Delta E_{\text{HYDR}}$  value for caffeine.

**Table 2.** Calculated values of the hydration energy ( $\Delta E_{\text{HYDR}}$ ), A<sub>2A</sub>AR interaction energy ( $\Delta E_{\text{INT}}$ ), and the overall receptor binding energy ( $\Delta E_{\text{BIND}}$ ) for caffeine and istradefylline, as well as relative deuteration-induced changes in the  $\Delta E_{\text{BIND}}$  as obtained by three different approaches explained in the Computational Details section (in kcal mol<sup>-1</sup>). The experimentally determined  $\Delta G_{\text{BIND,EXP}}$  are taken from refs. 31,32.

CAFFEINE				ISTRADEFYLLINE		
						
	ONIOM[1] <sup>1</sup>	ONIOM[2] <sup>2</sup>	DLPNO-CCSD(T) <sup>3</sup>	ONIOM[1] <sup>1</sup>	ONIOM[2] <sup>2</sup>	DLPNO-CCSD(T) <sup>3</sup>
$\Delta E_{\text{HYDR}}$		-43.5	-22.6		-13.0	-25.7
$\Delta E_{\text{INT}}$	/	-51.1	-32.5	/	-31.6	-43.4
$\Delta E_{\text{BIND}}$		-7.6	-9.9		-18.6	-17.7
Deuterated position	Deuteration-induced changes, $\Delta\Delta E_{\text{BIND}}$					
<b>1</b>	-0.1	-0.1	0.0	-0.2	-0.2	-0.2
<b>3</b>	-0.1	-0.2	-0.1	-0.1	-0.1	-0.1
<b>7</b>	-0.1	-0.1	0.0	0.0	-0.1	0.0
<b>1, 3, 7</b>	-0.3	-0.4	-0.2	-0.2	-0.3	-0.3
<b>1, 3</b>	-0.2	-0.3	-0.1	-0.2	-0.2	-0.3
<b>1, 7</b>	-0.2	-0.2	-0.1	-0.1	-0.2	-0.2
<b>3, 7</b>	-0.2	-0.1	-0.1	-0.1	-0.1	-0.1
<b>3'</b>				-0.3	0.0	0.0
<b>4'</b>				-0.3	-0.1	-0.2
<b>3', 4'</b>				-0.4	-0.4	-0.2
<b>POLY-D</b>				-0.6	-0.6	-0.5

<sup>1</sup> QM region: antagonist on the M06-2X/6-31+G(d) level; MM region: the rest of the system on the AMBER level

<sup>2</sup> QM region: antagonist, 5 the most dominant amino acid residues and 3 water molecules on the M06-2X/6-31+G(d) level; MM region: the rest of the system on the AMBER level

<sup>3</sup> (CPCM) DLPNO-CCSD(T)/cc-pVTZ//M06-2X/6-31+G(d) QM-only calculations on the cluster from the ONIOM[2] model

On the other hand, when the interaction efficiency of both ligands with the binding site residues is concerned,  $\Delta E_{\text{INT}}$  are consistently higher than  $\Delta E_{\text{HYDR}}$ , which confirms ligand ability to leave the aqueous solution and enter the receptor. In addition, within the ONIOM[2] approach, interaction energies  $\Delta E_{\text{INT}}$  are drastically, 38% higher for caffeine (-51.1 kcal mol<sup>-1</sup>) over -31.6 kcal mol<sup>-1</sup> calculated for istradefylline. This can appear misleading as, based on this aspect alone, one could expect a higher overall caffeine affinity, which is not the case. Instead, when taken together, it turns out, interestingly, that the higher istradefylline affinity predominantly originates in its much poorer water solvation prior to entering the receptor binding site. In other words, it seems that istradefylline is less comfortable in the aqueous solution, which is relieved once it finds its way into the receptor interior.

This motivated us to take a closer look into these aspects from MD simulations and record the number of relevant hydrogen bonding contacts with water molecules for each ligand in both phases (Table 3). Interestingly, although the unsaturated N9 nitrogen represents the most basic caffeine site,<sup>53</sup> it is significantly less hydrated than its carbonyl oxygens O11 and O13. While for the latter, the results indicate a permanent location of one water molecule around both oxygen sites, for N9 this occurs in only around half of structures (46%). In istradefylline, both O11 and O13 retain such a solvation pattern, while the N9 solvation is even further lower, where it takes place in every fifth structure (20%) that contributes to the lower overall ligand hydration. When both ligands are located within their A<sub>2A</sub>R binding positions, the proportion of direct ligand-water hydrogen bonding contacts drops significantly, since these are replaced by ligand-receptor interactions. This is manifested in all three relevant positions (N9, O11, O13), especially at the O13 site in istradefylline, where it is overtaken by an almost permanent O13...Asn253<sup>6,55</sup> contacts (86% of structures, Figure S9) that dominates its binding. As an even more illustrative example, we note that the istradefylline N9 site experiences no direct water contacts within the A<sub>2A</sub> binding site, being entirely surrounded by the receptor residues. Lastly, when both methoxy oxygens O3' and O4' are inspected, it appears that they retain their hydrogen bonding ability in both phases, as their cumulative effect assumes between 56–58% in both environments, which is not surprising given their exposure to the surrounding solvent water molecules even in the ligand bound state.

**Table 3.** The percentage of hydrogen bonding contacts with water molecules during MD simulations in the aqueous solution and A<sub>2A</sub> adenosine receptor, involving selected positions on both antagonists, calculated based on the total number of structures in individual simulations, 150.000 in water and 300.000 in the receptor.

	Caffeine		Istradefylline	
Position	Water	A <sub>2A</sub> receptor	Water	A <sub>2A</sub> receptor
N9	46%	20%	20%	0%
O11	96%	38%	92%	40%
O13	103%	85%	103%	14%
O3'	–	–	43%	32%
O4'	–	–	13%	26%

The focus of our work resides in estimating the effect of the selective deuteration on the affinity of both ligands and whether this bears any significance for potential clinical applications. When ONIOM[1] data are considered, we can observe that deuterium substitution is predominantly accompanied by a small, but genuine increase in affinity, which is encouraging. For caffeine, the results are even additive, which further supports its consideration as a reference molecule in this work. Specifically, trideuteration of a single methyl group in each of the three nitrogen sites, increases the overall affinity by  $-0.1$  kcal mol<sup>-1</sup>, meaning that all three *d*<sub>3</sub>-caffeine derivatives share the same increased potency towards the A<sub>2A</sub> receptor. Along these lines, when their *d*<sub>6</sub>-analogues are considered, each bearing two of its methyl group deuterated, the affinities consistently increase by  $-0.2$  kcal mol<sup>-1</sup>. Lastly, when the perdeuterated *d*<sub>9</sub>-derivative is concerned, with all

three methyl sites fully deuterated, the resulting caffeine affinity is increased by  $-0.3 \text{ kcal mol}^{-1}$ . This is both significant, since this affinity difference translates to around 1.7-fold increase in the potency, and applicable to various areas, from medicine to coffee and energy drink production. Namely, caffeine as a substance in food has long been utilised for its various physiological effects; primarily, increased alertness and mental performance with decreased fatigue, over its undesirable effects that may occur upon overconsumption, including insomnia, anxiety, tachycardia, and an increased blood pressure.<sup>54</sup> These effects are hypothesised to be driven by caffeine's downstream metabolites,<sup>55</sup> and our findings reveal that selective deuteration at any of its *N*-alkyl sites, let alone all three of them, could mitigate these undesirable outcomes, while improving the positive effects of the caffeine consumption. Accordingly, our results are found in line with reports demonstrating that the half-life of the perdeuterated  $d_9$ -caffeine following oral administration to rats increases 3 times in both plasma and the brain,<sup>12</sup> suggesting that despite an obvious reduction in the lipophilicity associated with deuteration,  $d_9$ -caffeine freely crossed the blood-brain barrier as its non-deuterated analogue. Taken together, this underlines a relevant and very interesting case when the selective deuteration exhibits positive and desirable effects on the ligand potency and its metabolic stability at the same time, which can be easily harnessed towards its improved therapeutic potential.

The magnitude of the calculated effect,  $\Delta\Delta E_{\text{BIND}} = -0.3 \text{ kcal mol}^{-1}$  for the  $d_9$ -derivative, deserves a few comments. Although, at first sight, this appears small and insignificant, the fact that it translates to around 1.7-fold potency increase bears significant pharmacological consequences and reveals a notable potential of deuterated drugs. Such a small effect is expected, knowing that our earlier experiments on the fully  $D_2O$ -incubated histamine  $H_2$  receptor,<sup>26</sup> when all acidic X-H bonds within the receptor and the ligand are exchanged to X-D, offered an increase in the histamine affinity of  $\Delta\Delta E_{\text{BIND}} = -0.75 \text{ kcal mol}^{-1}$ , thereby confirming that the effect exerted on only nine caffeine C-H bonds should be smaller. Also, Cherrah and co-workers used gas chromatography/mass spectrometry to investigate the affinity of caffeine and several of its deuterated isotopomers towards the human serum albumin and observed that all deuterium-enriched derivatives are linked with slightly lower affinities that stretch between  $81 \text{ M}^{-1}$  ( $\Delta\Delta G_{\text{BIND}} = 0.1 \text{ kcal mol}^{-1}$ ) and  $219 \text{ M}^{-1}$  ( $\Delta\Delta G_{\text{BIND}} = 0.4 \text{ kcal mol}^{-1}$ ) in the matching  $K_a$  values (Table S4).<sup>24</sup> In addition, based on a recent pharmacokinetic study in rats and *in vitro* human adenosine receptor models, Parente and co-workers measured  $IC_{50}$  values and demonstrated that the perdeuterated  $d_9$ -caffeine maintains the same receptor subtype preference ( $A_{2A} > A_{2B} > A_1 > A_3$ ), however, without providing an unequivocal conclusion about the effect on affinity.<sup>12</sup> Namely, although their reported concentration-response curves show significant overlap for the remaining three receptor subtypes, the one presented for the  $A_{2A}$  subtype reveals untypical shapes with the largest measurement confidence intervals among subtypes, hinting at a lower affinity at very small  $d_9$ -caffeine concentrations (including the zero inhibition), and an increased affinity at concentration exceeding  $50 \mu\text{M}$ . This led authors to conclude that " $d_9$ -caffeine is likely to exhibit an essentially identical, but prolonged, physiologic effect as compared to an equivalent dose of the non-deuterated caffeine", but we believe their report confirms our conclusion. Lastly, a very recent work by Hang Lai, Toussaint et al.<sup>31</sup> presented a development of an improved *in vivo* PET imaging of the brain  $A_{2A}$  receptor using [ $^{18}\text{F}$ ]FLUDA, a metabolically stable radiotracer with four methylene C-D bonds, whose  $A_{2A}R$  affinity is by  $-0.1 \text{ kcal mol}^{-1}$  higher than that of its non-deuterated [ $^{18}\text{F}$ ]FESCH. All of this gives us confidence to the validity of our calculations and the trends in the  $A_{2A}R$  affinity following caffeine deuteration.

Istradefylline is a larger system containing two additional sites inspected for deuteration, O3' and O4' methoxy group, together with a change from perdeuterated  $d_3$ -methyl moieties at sites N1 and N3 to perdeuterated  $d_5$ -ethyl units. Although istradefylline shares a certain partial structural similarity with caffeine, the results presented so far have clearly indicated notable differences in their features. Along these

lines, the only conserved site amenable to deuteration, the N7-methyl group, reveals no sensitivity to the isotope substitution whereas the same site in caffeine showed  $\Delta\Delta E_{\text{BIND}} = -0.1 \text{ kcal mol}^{-1}$ , while istradefylline, although associated with a more unique binding pose, reveals no additive trends in the selective site deuteration. Among the three xanthine nitrogen sites, N1-ethyl deuteration seems to exert a somewhat larger effect relative to other positions, which holds even in polydeuterated derivatives that include  $d_5$ -ethyl at the N1 position. Yet, when the entire xanthine part is polydeuterated, as in  $d_{13}$ -istradefylline, although containing four D-atoms more than in the analogous caffeine derivative, the overall effect on the affinity is smaller at  $\Delta\Delta E_{\text{BIND}} = -0.2 \text{ kcal mol}^{-1}$ , while it was  $\Delta\Delta E_{\text{BIND}} = -0.3 \text{ kcal mol}^{-1}$  in caffeine. Still, a very heartening insight is offered through both methoxy units, where the effect on any of them already matches the entire affinity increase in  $d_9$ -caffeine at  $\Delta\Delta E_{\text{BIND}} = -0.3 \text{ kcal mol}^{-1}$ . We find this very encouraging, since the synthetic efforts to introduce deuteration at O3' and O4' methoxy groups are somewhat simpler than within the xanthine core.<sup>56</sup> Even more so, not only that both methoxy substituents show identical response to deuteration, when they are jointly deuterated as in the corresponding  $d_6$ -istradefylline, the overall effect increases to  $\Delta\Delta E_{\text{BIND}} = -0.4 \text{ kcal mol}^{-1}$ , which surpasses caffeine and indicates a twice larger potency over non-deuterated istradefylline. All of this points to a conclusion that deuteration has a slightly larger effect on the 3,4-dimethoxyphenyl core over the xanthine part, which could be useful in guiding the design of new antagonists. This could be explained by the fact the structural variations in that part of the molecule, in the sense of introducing new groups or changing physico-chemical properties, have a more significant impact on the affinity than modification of the xanthine moiety, since they can affect the way how ligands occupy subsidiary binding sites outside the orthosteric pocket.<sup>40,49</sup> At last, when the polydeuterated  $d_{19}$ -istradefylline is considered, the improvement in the affinity further increases to  $\Delta\Delta E_{\text{BIND}} = -0.6 \text{ kcal mol}^{-1}$ , which translates to a 2.8-fold potency increase in such analogue relative to the unlabelled drug (Table 2, ONIOM[1] entries). Although one cannot neglect the synthetic challenges and difficulties associated with the preparation of this derivative, the obtained results strongly promote deuteration as a viable tool to advance istradefylline and, perhaps, other  $A_{2A}$ R antagonists, towards more potent and longer-lasting drugs. It is in this context that we bring this research into the focus of the interested industries and highly advise experimental efforts to confirm our observations.

## CONCLUSIONS

We developed an efficient and accurate computational methodology to address the effect of the selective deuteration on the receptor-ligand affinities, which relies on the ONIOM QM/MM calculations and the implicit quantisation of the nuclear motions. Although the impact of this work is broader and can be directly applied to any biological system, here we focused on the adenosine  $A_{2A}$  receptor antagonist istradefylline and its improved potency following the deuteration of various *N*- and *O*-alkyl groups, which was discussed relative to its structural analogue caffeine, a well-known and likely the most widely used stimulant. The devised approach treats the entire ligand at the QM level, while the rest of the ligand environment, whether the pure aqueous solution or the hydrated receptor structure, is accounted through the MM force field description. In our case, this led to the M06-2X/6-31+G(d):AMBER level of theory, whose validity was confirmed through (i) analogous ONIOM calculations with an extended QM region that included five active site residues most dominant for the binding, and three active site water molecules in direct hydrogen bonding contacts with ligands, and (ii) DLPNO-CCSD(T) local coupled cluster calculations within the same QM-only system, referred to as a "gold standard" quantum-chemical approach.<sup>57</sup> The starting point for these calculations was based on extracting representative structures following the unbiased docking and molecular dynamics simulations, while the isotope substitution is implicitly introduced through shortening of the

relevant C–H bonds by 3% and keeping them frozen during the optimisation of all other geometry parameters. Given that our primary model is most straightforward and does not critically depend on ambiguities in dividing the protein structure between QM/MM regions, we propose that this computational strategy can be safely used in the future research for the most efficient assessment of the binding isotope effect – a very promising tool to advance the existing drugs towards more potent and metabolically more stable compounds that is gaining in popularity in the medicinal and pharmaceutical chemistry over the years.

We note that our model relies on assuming identical binding orientations of deuterated and non-deuterated analogues, while changes in the lipophilicity and volume within the isotopically altered ligand could potentially modify its binding pose. Still, as presented in the Computational Details section, we do not have a computational methodology at hand to address this explicitly, especially while pertaining to the ligand-protein interactions involving large biological systems. Instead, we rely on numerous experiments that are consistent in reporting very small changes in the measured affinities upon isotope substitution,<sup>24,26,31</sup> or demonstrate a very similar adenosine receptor antagonist potency of *d*<sub>9</sub>-caffeine over caffeine,<sup>12,13</sup> which all suggest that the binding orientation among isotopomers is likely mostly preserved.

Our analysis showed that caffeine exhibits a pronounced flexibility within the A<sub>2A</sub> receptor and exchanges between two distinct binding poses that are found in agreement with crystallographic data. Although this allows caffeine to optimise its contacts with the active site residues, most of its interactions are based on weak hydrophobic contacts and not on stronger hydrogen bonding interactions, which might be anticipated given its polar and heteroaromatic structure with several potential hydrogen bonding acceptor sites. This leads to a lower affinity over istradefylline, and our ONIOM predicted value of  $-7.6 \text{ kcal mol}^{-1}$  is found in an almost perfect agreement with  $-7.7 \text{ kcal mol}^{-1}$  measured experimentally. On the other hand, the additional C8-*trans*-styryl fragment in istradefylline serves the effect of locking the ligand within a uniform pose, while contributing to the binding through the C–H $\cdots\pi$  and  $\pi\cdots\pi$  interactions with residues closer to the surface entrance. This, together with a much less favourable hydration prior to binding, enhances the affinity relative to caffeine. In both cases, the ligand-receptor recognition is dominated by Phe168, Leu249, Asn253, Leu249 and Met270 residues, as elucidated through the MM-GBSA analysis, which agrees with earlier literature reports and confirms the hydrophobic character of the binding site, thereby underlying important guidelines for the future design of potent A<sub>2A</sub> receptor antagonists.

Caffeine reveals higher consistency and additive effects following its deuteration in a way that any deuterated *N*-methyl moiety enhances the affinity by  $-0.1 \text{ kcal mol}^{-1}$ , which culminates in the perdeuterated *d*<sub>9</sub>-caffeine having by  $-0.3 \text{ kcal mol}^{-1}$  higher A<sub>2A</sub>R affinity than its non-deuterated analogue. This translates to around 1.7-fold potency increase, which is likely relevant for its pharmaceutical implementations, but also for the application in the industries related to the coffee and energy drinks production.

On the other hand, istradefylline displays a much higher deuteration sensitivity within its C8-*trans*-styryl unit, where the effect following the isotope substitution in both of its methoxy positions, *d*<sub>6</sub>-istradefylline, already surpasses that of the perdeuterated *d*<sub>9</sub>-caffeine, and assumes  $\Delta\Delta E_{\text{BIND}} = -0.4 \text{ kcal mol}^{-1}$ . However, the full potential of this strategy is achieved in the polydeuterated *d*<sub>19</sub>-istradefylline, whose affinity towards the A<sub>2A</sub> receptor improves by  $\Delta\Delta E_{\text{BIND}} = -0.6 \text{ kcal mol}^{-1}$ , thereby indicating a 2.8-fold potency increase, thus motivating us to suggest this as a potential target for synthetic organic researchers.

Lastly, let us emphasise that our results provide convincing support that the H/D exchange within alkyl moieties in caffeine and istradefylline is accompanied by the A<sub>2A</sub> adenosine receptor affinity increase, which is genuine and, despite its diminutiveness, may, in cases of polydeuterated ligands, have marked biological consequences considering the augmentation in binding strength by around two and three times,

respectively, relative to their parent non-deuterated compounds. This knowledge opens the door for the implementation of deuterium in the development of new drugs which could, besides its effect on the affinity, positively modify cumulative clinical profiles of the already marketed substances. Nevertheless, the impact on pharmacokinetics, metabolism, safety profiles and human inter-individual differences of these polydeuterated antagonists have yet to be extensively investigated. Still, the success of the clinically approved deutetrabenazine (Austedo) and deucravacitinib (Sotyktu) has given industry the confidence to invest in the expansion of deuterated drugs. As a result, more than 20 deuterated drugs are currently in the clinical development, with several of them having reached Phase III clinical trials,<sup>7</sup> while it is easily foreseen that a number of them will follow these examples and hit the market in the years to come.

## **FUNDING**

This work was supported by CAT PHARMA (KK.01.1.1.04.0013), a project co-financed by the Croatian Government and the European Union through the European Regional Development Fund – the Competitiveness and Cohesion Operational Programme.

## **DATA AND SOFTWARE AVAILABILITY**

Universal Protein Resource database (<https://www.uniprot.org/>), SWISS-MODEL homology modelling tool (<https://swissmodel.expasy.org/>), ERRAT tool and PROCHECK tool (<https://saves.mbi.ucla.edu/>), PROPKA 3.1 (<https://server.poissonboltzmann.org/pdb2pqr>), Amber16 and AmberTools16 (<https://ambermd.org/>), CHARMM-GUI web server (<https://www.charmm-gui.org/>), PPM web server ([https://opm.phar.umich.edu/ppm\\_server](https://opm.phar.umich.edu/ppm_server)), AutoDock Vina program and AutoGrid program (<https://vina.scripps.edu/>), UCSF Chimera 1.16. (<https://www.cgl.ucsf.edu/chimera/>), CREST tool (<https://crest-lab.github.io/crest-docs/>), Gaussian16 software (<https://gaussian.com/>), ORCA software (<https://sites.google.com/site/orcainputlibrary/home>), TAO package (<http://schlegelgroup.wayne.edu/Software/oniomtoolTAO/TAOtutorial.html>).

All data to reproduce theoretical calculations are included in Supporting Information. The data (MD trajectories) obtained in this work and the in-house scripts can be obtained from the authors of the manuscript upon request.

## **SUPPORTING INFORMATION**

Computational details, various graphical and tabular analyses from docking and MD simulations, and Cartesian coordinates for systems reported in the paper (PDF).

## **ACKNOWLEDGMENTS**

L.H. acknowledges the Croatian Science Foundation for a doctoral stipend through the Career Development Project for Young Researchers (DOK-2020-01-3482). We are grateful to the Zagreb University Computing Centre for granting computational resources on the ISABELLA cluster. We thank Luka Bilić, Dr. Zlatko Brkljača and Dr. Davor Šakić for their assistance with ONIOM and ORCA calculations.



## CONFLICT OF INTEREST DISCLOSURE

The authors declare no competing financial interest.

## REFERENCES

1. Cheng, R.K.Y.; Segala, E.; Robertson, N.; Deflorian, F.; Doré, A.S.; Errey, J.C.; Fiez-Vandal, C.; Marshall, F.H.; Cooke, R.M. Structures of Human A<sub>1</sub> and A<sub>2A</sub> Adenosine Receptors with Xanthines Reveal Determinants of Selectivity. *Structure* **2017**, *25*, 1275–1285.
2. Topiol, S. Current and Future Challenges. In: Heifetz, A. (ed.), *GPCR Drug Discovery in Computational Methods for GPCR Drug Discovery*. New York: Springer Nature, 2018, 1–23.
3. Ciancetta, A.; Jacobson, K.A. Breakthrough in GPCR Crystallography and Its Impact on Computer-Aided Drug Design. In: Heifetz, A. (ed.), *GPCR Drug Discovery in Computational Methods for GPCR Drug Discovery*. New York: Springer Nature, 2018, 45–72.
4. Jenner, P.; Mori, A.; Aradi, S.D.; Hauser, R.A. Istradefylline - a first generation adenosine A<sub>2A</sub> antagonist for the treatment of Parkinson's disease. *Expert Rev Neurother* **2021**, *21*, 317–333.
5. Chen, J.F.; Eltzhig, H.; Fredholm, B. Adenosine receptors as drug targets — what are the challenges? *Nat Rev Drug Discov* **2013**, *12*, 265–286.
6. Shook, B.C.; Jackson, P.F. Adenosine A<sub>2A</sub> Receptor Antagonists and Parkinson's Disease. *ACS Chem Neurosci* **2011**, *2*, 555–567.
7. Pirali, T.; Serafini, M.; Cargnin, S.; Genazzani, A.A. Applications of Deuterium in Medicinal Chemistry. *J Med Chem* **2019**, *62*, 5276–5297.
8. Austedo Dosage, 2022. Available from: <https://www.drugs.com/dosage/austedo.html> [Accessed 13 Dec 2022].
9. Huntington Study Group; Frank, S.; Testa, C.M.; Stamler, D.; Kayson, E.; Davis, C.; Edmondson, M.C.; Kinel, S.; Leavitt, B.; Oakes, D.; O'Neill, C.; Vaughan, C.; Goldstein, J.; Herzog, M.; Snively, V.; Whaley, J.; Wong, C.; Suter, G.; Jankovic, J.; Jimenez-Shahed, J.; Hunter, C.; Claassen, D.O.; Roman, O.C.; Sung, V.; Smith, J.; Janicki, S.; Clouse, R.; Saint-Hilaire, M.; Hohler, A.; Turpin, D.; James, R.C.; Rodriguez, R.; Rizer, K.; Anderson, K.E.; Heller, H.; Carlson, A.; Criswell, S.; Racette, B.A.; Revilla, F.J.; Nucifora, F. Jr.; Margolis, R.L.; Ong, M.; Mendis, T.; Mendis, N.; Singer, C.; Quesada, M.; Paulsen, J.S.; Brashers-Krug, T.; Miller, A.; Kerr, J.; Dubinsky, R.M.; Gray, C.; Factor, S.A.; Sperin, E.; Molho, E.; Eglow, M.; Evans, S.; Kumar, R.; Reeves, C.; Samii, A.; Chouinard, S.; Beland, M.; Scott, B.L.; Hickey, P.T.; Esmail, S.; Fung, W.L.; Gibbons, C.; Qi, L.; Colcher, A.; Hackmyer, C.; McGarry, A.; Klos, K.; Gudesblatt, M.; Fafard, L.; Graffitti, L.; Schneider, D.P.; Dhall, R.; Wojcieszek, J.M.; LaFaver, K.; Duker, A.; Neefus, E.; Wilson-Perez, H.; Shprecher, D.; Wall, P.; Blindauer, K.A.; Wheeler, L.; Boyd, J.T.; Houston, E.; Farbman, E.S.; Agarwal, P.; Eberly, S.W.; Watts, A.; Tariot, P.N.; Feigin, A.; Evans, S.; Beck, C.; Orme, C.; Edicola, J.; Christopher, E. Effect of Deutetrabenazine on Chorea Among Patients With Huntington Disease. A Randomized Clinical Trial. *JAMA* **2016**, *316*, 40–50.

10. U.S. Food and Drug Administration Approves Sotyktu™ (deucravacitinib), Oral Treatment for Adults with Moderate-to-Severe Plaque Psoriasis, 2022. Available from: <https://news.bms.com/news/details/2022/U.S.-Food-and-Drug-Administration-Approves-Sotyktu-deucravacitinib-Oral-Treatment-for-Adults-with-Moderate-to-Severe-Plaque-Psoriasis/default.aspx> [Accessed 5 Jan 2023].
11. Wroblewski, S.T.; Moslin, R.; Lin, S.; Zhang, Y.; Spengel, S.; Kempson, J.; Tokarski, J.S.; Strnad, J.; Zupa-Fernandez, A.; Cheng, L.; Shuster, D.; Gillooly, K.; Yang, X.; Heimrich, E.; McIntyre, K.W.; Chaudhry, C.; Khan, J.; Ruzanov, M.; Tredup, J.; Mulligan, D.; Xie, D.; Sun, H.; Huang, C.; D'Arienzo, C.; Aranibar, N.; Chiney, M.; Chimalakonda, A.; Pitts, W.J.; Lombardo, L.; Carter, P.H.; Burke, J.R.; Weinstein, D.S. Highly Selective Inhibition of Tyrosine Kinase 2 (TYK2) for the Treatment of Autoimmune Diseases: Discovery of the Allosteric Inhibitor BMS-986165. *J Med Chem* **2019**, *62*, 8973–8995.
12. Parente, R.M.; Tarantino, P.M.; Sippy, B.C.; Burdock, G.A. Pharmacokinetic, pharmacological, and genotoxic evaluation of deuterated caffeine. *Food Chem Toxicol* **2022**, *160*, 112774.
13. Sherman, M.M.; Tarantino, P.M.; Morrison, D.N.; Lin, C.-H.; Parente, R.M.; Sippy, B.C. A double-blind, randomized, two-part, two-period crossover study to evaluate the pharmacokinetics of caffeine versus *d*<sub>9</sub>-caffeine in healthy subjects. *Regul. Toxicol. Pharmacol.* **2022**, *133*, 105194.
14. Meanwell, N.A. Synopsis of Some Recent Tactical Application of Bioisosteres in Drug Design. *J Med Chem* **2011**, *54*, 2529–2591.
15. Guengerich, F.P. Kinetic deuterium isotope effects in cytochrome P450 reactions. *Methods Enzymol* **2017**, *596*, 217–238.
16. Vianello, R.; Repič, M.; Mavri, J. How are Biogenic Amines Metabolized by Monoamine Oxidases? *Eur J Org Chem* **2012**, *2012*, 7057–7065.
17. Poberžnik, M.; Purg, M.; Repič, M.; Mavri, J.; Vianello, R. Empirical Valence Bond Simulations of the Hydride-Transfer Step in the Monoamine Oxidase A Catalyzed Metabolism of Noradrenaline. *J Phys Chem B* **2016**, *120*, 11419–11427.
18. Prah, A.; Purg, M.; Stare, J.; Vianello, R.; Mavri, J. How Monoamine Oxidase A Decomposes Serotonin: An Empirical Valence Bond Simulation of the Reactive Step. *J Phys Chem B* **2020**, *124*, 8259–8265.
19. Kargbo, R.B. Application of Deuterated N,N-Dimethyltryptamine in the Potential Treatment of Psychiatric and Neurological Disorders. *ACS Med Chem Lett* **2022**, *13*, 1402–1404.
20. Świderek, K.; Paneth, P. Binding Isotope Effects. *Chem Rev* **2013**, *113*, 7851–7879.
21. Bechalany, A.; El Tayar, N.; Carrupt, P.-A.; Testa, B.; Falconnet, J.-B.; Cherrah, Y.; Benchekroun, Y.; Brazier, J.-L. Isotope Effects on the Lipophilicity of Deuterated Caffeines. *Helv Chim Acta* **1989**, *72*, 472–476.
22. Falconnet, J.B.; Brazier, J.L.; Desage, M. Synthesis of seven deuteromethyl-caffeine analogues; observation of deuterium isotope effects on CMR analysis. *J Label Compd Radiopharm* **1986**, *23*, 267–276.
23. Brazier, J.L.; Ribon, B.; Falconnet, J.B.; Cherrah, Y.; Benchekroun, Y. Etude et utilisation des effets isotopiques en pharmacologie. *Therapie* **1987**, *42*, 445–450.

24. Cherrah, Y.; Falconnet, J.B.; Desage, M.; Brazier, J.L.; Zini, R.; Tillement, J.P. Study of deuterium isotope effects on protein binding by gas chromatography/mass spectrometry. Caffeine and deuterated isotopomers. *Biomed Environm Mass Spectrom* **1987**, *14*, 653–657.
25. Cherrah, Y.; Zini, R.; Falconnet, J.B.; Desage, M.; Tillement, J.P.; Brazier, J.L. Study of deuterio-isotopomer-induced inhibition of caffeine and phenobarbitone binding to human serum albumin. *Biochem Pharmacol* **1988**, *37*, 1311–1315.
26. Hok, L.; Mavri, J.; Vianello, R. The effect of deuteration on the H<sub>2</sub> receptor histamine binding profile: A computational insight into modified hydrogen bonding interactions. *Molecules* **2020**, *25*, 6017.
27. Kržan, M.; Keuschler, J.; Mavri, J.; Vianello, R. Relevance of Hydrogen Bonds for the Histamine H<sub>2</sub> Receptor-Ligand Interactions: A Lesson from Deuteration. *Biomolecules* **2020**, *10*, 196.
28. de Lera Ruiz, M.; Lim, Y.-H.; Zheng, J. Adenosine A<sub>2A</sub> Receptor as a Drug Discovery Target. *J Med Chem* **2014**, *57*, 3623–3650.
29. Mori, A.; Chen, J.-F.; Uchida, S.; Durlach, C.; King, S.M.; Jenner, P. The Pharmacological Potential of Adenosine A<sub>2A</sub> Receptor Antagonists for Treating Parkinson's Disease. *Molecules* **2022**, *27*, 2366.
30. Wang, Y.; Wang, H.; Xu, H.; Zheng, Z.; Meng, Z.; Xu, Z.; Li, J.; Xue, M. Design and synthesis of five-membered heterocyclic derivatives of istradefylline with comparable pharmacological activity. *Chem Biol Drug Des* **2022**, *100*, 534–552.
31. Lai, T.H.; Toussaint, M.; Teodoro, R.; Dukić-Stefanović, S.; Gündel, D.; Ludwig, F.-A.; Wenzel, B.; Schröder, S.; Sattler, B.; Moldovan, R.-P.; Falkenburger, B.H.; Sabri, O.; Deuther-Conrad, W.; Brust, P. Improved in vivo PET imaging of the adenosine A<sub>2A</sub> receptor in the brain using [<sup>18</sup>F]FLUDA, a deuterated radiotracer with high metabolic stability. *Eur J Nucl Med Mol Imaging* **2021**, *48*, 2727–2736.
32. Haanes, K.A.; Edvinsson, L. Expression and Characterization of Purinergic Receptors in Rat Middle Meningeal Artery—Potential Role in Migraine. *PLoS ONE* **2014**, *9*, e108782.
33. Akbar, S.; Mozumder, S.; Sengupta, J. Retrospect and prospect of single particle cryo-electron microscopy: The class of integral membrane proteins as an example. *J Chem Inf Model* **2020**, *60*, 2448–2457.
34. van Meer, G.; Voelker, D.R.; Feigenson, G.W. Membrane lipids: where they are and how they behave. *Nat Rev Mol Cell Biol* **2008**, *9*, 112–124.
35. Ackerman, D.G.; Feigenson, G.W. Lipid bilayers: clusters, domains and phases. *Essays Biochem* **2015**, *57*, 33–42.
36. Dawaliby, R.; Trubbia, C.; Delporte, C.; Masureel, M.; Van Antwerpen, P.; Kobilka, B.K.; Govaerts, C. Allosteric regulation of G protein-coupled receptor activity by phospholipids. *Nat Chem Biol* **2016**, *12*, 35–39.
37. Bruzzese, A.; Gil, C.; Dalton, J.A.R.; Giraldo, J. Structural insights into positive and negative allosteric regulation of a G protein-coupled receptor through protein-lipid interactions. *Sci Rep* **2018**, *8*, 4456.
38. Wakefield, A. E.; Bajusz, D.; Kozakov, D.; Keserű, G. M.; Vajda, S. Conservation of allosteric ligand binding sites in G-protein coupled receptors. *J Chem Inf Model* **2022**, *62*, 4937–4954.

39. Segala, E.; Guo, D.; Cheng, R.K.Y.; Bortolato, A.; Deflorian, F.; Doré, A.S.; Errey, J.C.; Heitman, L.H.; IJzerman, A.P.; Marshall, F.H.; Cooke, R.M. Controlling the Dissociation of Ligands from the Adenosine A<sub>2A</sub> Receptor through Modulation of Salt Bridge Strength. *J Med Chem* **2016**, *59*, 6470–6479.
40. Carpenter, B.; Lebon, G. Human Adenosine A<sub>2A</sub> Receptor: Molecular Mechanism of Ligand Binding and Activation. *Front Pharmacol* **2017**, *8*, 898.
41. Lebon, G.; Warne, T.; Edwards, P.C.; Bennett, K.; Langmead, C.J.; Leslie, A.G.W.; Tate, C.G. Agonist-bound adenosine A<sub>2A</sub> receptor structures reveal common features of GPCR activation. *Nature* **2011**, *474*, 521–525.
42. Mattedi, G.; Deflorian, F.; Mason, J. S.; de Graaf, C.; Gervasio, F. L. Understanding ligand binding selectivity in a prototypical GPCR family. *J Chem Inf Model* **2019**, *59*, 2830–2836.
43. Woolley, M.J.; Watkins, H.A.; Taddese, B.; Karakullukcu, Z.G.; Barwell, J.; Smith, K.J.; Hay, D.L.; Poyner, D.R.; Reynolds, C.A.; Conner, A.C. The role of ECL2 in CGRP receptor activation: a combined modelling and experimental approach. *J R Soc Interface* **2013**, *10*, 20130589.
44. Woolley, M.J.; Conner, A.C. Understanding the common themes and diverse roles of the second extracellular loop (ECL2) of the GPCR super-family. *Mol Cell Endocrinol* **2017**, *449*, 3–11.
45. Pang, X.; Yang, M.; Han, K. Antagonist binding and induced conformational dynamics of GPCR A<sub>2A</sub> adenosine receptor. *Proteins* **2013**, *81*, 1399–1410.
46. Tošović, J.; Fijan, D.; Jukič, M.; Bren, U. Conserved water networks identification for drug design using density clustering approaches on positional and orientational data. *J Chem Inf Model* **2022**, *62*, 6105–6117.
47. Matricon, P.; Suresh, R.R.; Gao, Z.-G.; Panel, N.; Jacobson, K.A.; Carlsson, J. Ligand design by targeting a binding site water. *Chem Sci* **2021**, *12*, 960–968.
48. Bruzzese, A.; Dalton, J.A.R.; Giraldo, J. Insights into adenosine A<sub>2A</sub> receptor activation through cooperative modulation of agonist and allosteric lipid interactions. *PLoS Comput Biol* **2020**, *16*, e1007818.
49. Saini, A.; Patel, R.; Gaba, S.; Singh, G.; Gupta, G.D.; Monga, V. Adenosine receptor antagonists: Recent advances and therapeutic perspective. *Eur J Med Chem* **2022**, *227*, 113907.
50. Glukhova, A.; Thal, D.M.; Nguyen, A.T.; Vecchio, E.A.; Jörg, M.; Scammells, P.J.; May, L.T.; Sexton, P.M.; Christopoulos, A. Structure of the Adenosine A<sub>1</sub> Receptor Reveals the Basis for Subtype Selectivity. *Cell* **2017**, *168*, 867–877.
51. Maršavelski, A.; Vianello, R. What a Difference a Methyl Group Makes: The Selectivity of Monoamine Oxidase B Towards Histamine and *N*-Methylhistamine. *Chem Eur J* **2017**, *23*, 2915–2925.
52. Wang, Y.; Xu, H.; Wang, H.; Zheng, Z.; Meng, Z.; Xu, Z.; Li, J.; Xue, M. Design, Synthesis, and Biological Activity Studies of Istradefylline Derivatives Based on Adenine as A<sub>2A</sub> Receptor Antagonists, *ACS Omega* **2021**, *6*, 4386–4394.
53. Tshepelevitsh, S.; Kütt, A.; Lõkov, M.; Kaljurand, I.; Saame, J.; Heering, A.; Plieger, P.G.; Vianello, R.; Leito, I. On the basicity of organic bases in different media. *Eur J Org Chem* **2019**, 6735–6748.

54. van Dam, R.M.; Hu, F.B.; Willett, W.C. Coffee, Caffeine, and Health. *N Engl J Med* **2020**, *383*, 369–378.
55. Ribeiro, J.A.; Sebastião, A.M. Caffeine and adenosine. *J Alzheimers Dis* **2010**, *20 Suppl 1*, S3–S15.
56. Ding, H.X.; Leverett, C.A.; Kyne Jr, R.E.; Liu, K. K.-C.; Fink, S.J.; Flick, A.C.; O'Donnell, C.J. Synthetic approaches to the 2013 new drugs. *Bioorg Med Chem* **2015**, *23*, 1895–1922.
57. Ryde, U.; Söderhjelm, P. Ligand-Binding Affinity Estimates Supported by Quantum-Mechanical Methods, *Chem Rev* **2016**, *116*, 5520–5566.

FOR TABLE OF CONTENTS USE ONLY

## Selective Deuteration Improves the Affinity of Adenosine A<sub>2A</sub> Receptor Ligands – A Computational Case Study with Istradefylline and Caffeine

Lucija Hok and Robert Vianello\*

